LA-UR- 99-1341

Approved for public release;
distribution is unlimited.

Title: A Model for the Prediction of the Hydriding Thermodynamics of Pd-Rh-Co Ternary Alloys

Author(s): D. F. Teter, MST-6
D J. Thoma, MST-6

Submitted to: TSM '99 Annual Meeting
San Diego, California
3/1-4/99

Los Alamos
NATIONAL LABORATORY

DISCLAIMER

DISCLAIMER

Portions of this document may be illegible in electronic image products. Images are produced from the best available original document.

A Model for the Prediction of the Hydriding Thermodynamics of Pd-Rh-Co Ternary Alloys

D.F. Teter and D.J. Thoma

Materials Science and Technology Division, Los Alamos National Laboratory, Los Alamos, NM 87545

ABSTRACT

A dilute solution model (with respect to the substitutional alloying elements) has been developed, which accurately predicts the hydride formation and decomposition thermodynamics and the storage capacities of dilute ternary Pd-Rh-Co alloys. The effect of varying the rhodium and cobalt compositions on the thermodynamics of hydride formation and decomposition and hydrogen capacity of several palladium-rhodium-cobalt ternary alloys has been investigated using pressure-composition (PC) isotherms. Alloying in the dilute regime (<10 at. %) causes the enthalpy for hydride formation to linearly decrease with increasing alloying content. Cobalt has a stronger effect on the reduction in entahlpy than rhodium for equivalent alloying amounts. Also, cobalt reduces the hydrogen storage capacity with increasing alloying content. The plateau thermodynamics are strongly linked to the lattice parameters of the alloys. A near-linear dependence of the enthalpy of hydride formation on the lattice parameter was observed for both the binary Pd-Rh and Pd-Co alloys, as well as for the ternary Pd-Rh-Co alloys. The Pd-5Rh-3Co (at. %) alloy was found to have similar plateau thermodynamics as a Pd-10Rh alloy, however, this ternary alloy had a diminshed hydrogen storage capacity relative to Pd-10Rh.

1. Introduction

Historically, palladium-rhodium alloys have been attractive for hydrogen storage due to their fast kinetics, high storage capacities, and structural stability with hydrogen cycling. In particular, the storage capacity is maximized at about Pd-7 at. %Rh[1]. However, recent studies[2-5] have shown that hydrogen causes metastable Pd-Rh solid solutions to phase separate. The established Pd-Rh phase diagram shows a miscibility gap with a boundary of about 12 %Rh at 600°C[6-8]. No data exists delineating the boundary at lower temperatures because of the sluggish kinetics of the phase separation, but extrapolations to room temperature suggest that the boundary would be approximately Pd 5-7 at. % Rh. Therefore, Pd alloys containing greater than 5 %Rh are considered metastable and have the potential to undergo hydrogen-induced phase separation. Consequently this may produce an altered thermodynamic response over time. To ensure a reliable alloy with constant hydrogen absorption/desorption and hydriding/dehydriding thermodynamic properties over time, the alloy is required to be a stable solid solution, less than ~5 %Rh addition. Unfortunately, decreasing the Rh content also decreases the hydriding plateau pressures. Cobalt forms a solid solution with Pd up to about 10 at. % Co, above which, a metastable ordered $L1_2$ compound, $CoPd_3$, has been observed in thin films[9]. Cobalt also increases the plateau pressures[10,11]. Therefore with small additions of cobalt to a "lean" Rh alloy, it is possible to approach the thermodynamic properties and storage capacity of a Pd-7 at. % Rh alloy and still retain a stable solid solution which would not be susceptible to hydrogen-induced phase separation.

A multitude of literature exists describing the thermodynamics of binary Pd-based alloys. Unfortunately, the characterization of these alloys has been primarily limited to documenting the

thickness of the foils used. The actual compositions are rarely measured after processing. It is generally assumed that the alloys are of a nominal composition based upon weight of constituents prior to processing. Therefore, small discrepancies in the literature regarding the thermodynamic properties of hydride formation/dissolution in Pd-Rh alloys could be attributable to differences in actual alloy content. Similarly the interstitial content (B, C, N, O, S, P etc.) is rarely reported, and differences in the thermodynamic properties of the solution of hydrogen in Pd-Rh alloys could be attributed to the variations in interstitial content. Full characterization of a sample used for thermodynamic analysis is required in order to interpret subtleties in the data.

A few thermodynamic measurements have been made on ternary Pd-based alloys as well[12-14]. However, no attempts have been made to quantify the effects of alloying on the thermodynamic properties of these alloys for a predictive capability. In the design of alloys for hydrogen storage, it would be useful to develop an alloy with specific hydrogen absorption and hydriding thermodynamics. A predictive model is imperative to effectively and efficiently design a hydrogen storage alloy. Since the thermodynamic properties are strongly dependent on alloy content, purity, and other microstructural variables, many samples must be fully characterized to develop a model. In this work, a dilute solution model (with respect to the substitutional alloying elements) was developed which accurately predicts the hydride formation and decomposition thermodynamics and the storage capacities of dilute ternary Pd-Rh-Co alloys.

Cobalt was used as the ternary alloying element to improve alloy phase stability in the presence of hydrogen while still maintaining hydriding thermodynamic properties equivalent to the binary palladium-rhodium system. Binary Pd-Rh and Pd-Co alloys were produced with particular attention to purity and characterization to obtain good thermodynamic data used in the

prediction of the thermodynamics of the ternary Pd-Rh-Co alloys. The following sections describe the binary and ternary alloys examined, their properties and model predictions.

2. Experimental

In this study, two Pd-Rh binary alloys, three Pd-Co binary alloys, and four Pd-Rh-Co ternary alloys were prepared with the nominal compositions (at. %) of the alloys given in Table 1. Palladium (99.99%), rhodium (99.99%) and cobalt (99.99%) sponge powders were mixed and pressed (using no lubricants) into green compacts. These compacts were then arc-melted several times in an evacuated and argon purged chamber and cast into a "finger" form. This cast finger was then homogenized for 72 hours at 1200°C in an ultra-high purity Ar (99.999%) environment with a titanium getter. After homogenizing, the ingots were rolled to a thickness of about 100 μm. If cracking occurred during rolling, an intermediate anneal of 900°C for 2 hours was used. After cold rolling, all foils were annealed again at 900°C for 24 hours and slow cooled.

Pressure-composition (PC) isotherms were measured on a computer-automated Sievert's type apparatus using a water bath to maintain a constant sample temperature (± 0.1°C) during the measurements. Prior to inserting the samples into the Sievert's apparatus, the specimens were etched in an acid solution containing HNO_3, H_2SO_4 and H_2O at the ratio of 2:2:1, respectively, as done by Sakamoto et al.[15] to clean the surface. Specimens, weighing between 1 and 3 g, were loaded into the sample chamber and purged five times with ultra-high purity Ar. The hydrogen concentration was measured from a change in pressure of the system with a constant and known volume at constant temperature. The software program calculated the slope of the pressure-time curve and determined that equilibrium was reached when the slope over the last 20 min is less than 36 mtorr/hr. This is also verified by visual examination of the pressure-time curve for each

data point. The alloys were cycled a minimum of eight times at 50°C to ensure a stable PCT behavior. The same sample is then used to measure the PC response as a function of temperature.

Prior to PCT analysis, samples were examined by optical metallography to determine the homogeneity of the microstructure and grain size. Due to the size of the grains relative to the foil thickness, the typical ASTM grain size measurement technique could not be done. Therefore, the grain size was estimated by drawing several parallel lines perpendicular to the thickness of the foil. An intercept method was then used to determine the grain size. Measurements along the thickness of the foil were not made since the grains are fairly equiaxed, and in some cases, equal to the thickness of the foil. Micro-hardness measurements were also taken of the samples before PCT analysis. Lastly, x-ray diffraction of the annealed samples was performed with a Scintag x-ray diffractometer using Cu Kα radiation and a curved pyrolytic graphite monochromator. Lattice parameters were determined by plotting the lattice parameters for each diffraction peak against $\cos^2\theta/\sin\theta$ and extrapolating to $\cos^2\theta/\sin\theta=0$. This analysis gave good fits with the error in the lattice parameter less than or equal to 0.0004 Å. Luvak Inc. performed chemical analysis on samples after the samples had been used for the PCT measurements. All compositions in this work will be in atomic percent or appm unless otherwise stated. The rhodium and cobalt compositions were measured using plasma emission spectroscopy. Boron and phosphorus were measured using direct current plasma emission spectroscopy. Combustion-infrared detection was used to determine the carbon content; and oxygen and nitrogen were analyzed using the inert gas fusion technique. Sulfur was measured using a combustion-iodometric titration technique. All measurement techniques follow ASTM standards.

3. Results and Discussion

3.1 Characterization

The results, from metallographic examination of the foils, show large equiaxed grains with no evidence of alloy segregation due to dendrites. Previous experience with similar heat treatments has shown that no segregation is detectable using electron-probe microanalysis, which has a spatial resolution of about 1 μm. Examples of the microstructure of the foils are given in Figure 1. The alloy foils are typically 90-120 μm thick and have a grain size of about 50 μm. Measurements for all of the foils are given in Table 2. Only the Pd-5Rh alloy required a secondary anneal during the rolling process. This secondary anneal did not appreciably affect the grain size which was 65 μm for the Pd-5Rh alloy and 59 μm for the Pd-10Rh alloy.

The Vicker's hardness of the annealed alloys ranged from 62 to 83 with the higher alloyed samples having a higher hardness as would be expected from substitutional hardening, see Table 2. After cycling through the hydriding/dehydriding reactions several times, the hardnesses increased by about a factor of two relative to the annealed state due to the large amount of work hardening occurring during the formation and decomposition of hydrides. Overall, the low hardnesses of the annealed alloys correlate well with the high purity of the material as evidenced by the chemical analysis. Table 1 summarizes the chemical analysis of the alloys examined in this study. The analysis results of the rhodium and cobalt concentrations show that it is a poor assumption to use the nominal composition instead of the actual compositions, since in some cases the actual composition was > 0.5 at. % less than the nominal composition determined from weighing the powders. The only element consistently detectable above background was oxygen. Oxygen contents ranged from 46 to 244 appm (7 to 37 wppm).

The carbon concentrations were just slightly above the level of detectability except for the Pd-5Rh-1Co alloy, which had a carbon content of 2108 appm (40 wppm). This is still a low carbon content but may explain why the hardness of this alloy is slightly higher than Pd-5Rh-3Co when it would be expected to be lower due to lower total alloying content. Overall the interstitial content of these alloys is very low. Therefore, differences in the thermodynamics of hydrogen absorption and hydriding was attributed solely to the effect of Rh and Co additions.

X-ray diffraction measurements showed that all alloys are homogeneous, metastable face-centered cubic solid solutions. Lattice parameters for the alloys were calculated assuming a Vegard's law relationship between the pure elemental lattice parameters. For the case of cobalt which is hexagonally close-packed at room temperature, the lattice parameter of the high-temperature face-centered cubic structure was extrapolated to room temperature. Lattice parameters of cobalt show a linear dependence with temperature[16-18]. When extrapolated to 293 K, the lattice parameter is 3.540 Å. The pure rhodium lattice parameter, from Ross and Hume-Rothery[19], is 3.8032 Å. Pure Pd, measured in this work, has a lattice parameter of 3.8901 Å. Good agreement exists for the Pd-Rh binary alloys suggesting that the alloys behave as ideal solutions. The ternary Pd-Rh-Co alloys do not agree quite as well most likely due to the uncertainties in the extrapolated cobalt lattice parameter. However at a constant 5%Rh content, the lattice parameter does decrease linearly with increasing cobalt content as seen in Figure 2.

3.2 Thermodynamics

The pressure-composition-temperature curves are presented in Figure 3 through Figure 10 for the Pd-Rh and Pd-Co binary alloys and the Pd-Rh-Co ternary alloys. The alloys were cycled

eight times to ensure a repeatable pressure-composition behavior. Generally, the α-phase solvus increases, the plateau pressures increase, and the β-phase solvus decreases with increasing temperature. Neither the Pd-5Rh nor the Pd-10Rh alloys, Figure 3 and Figure 4, exhibit the anomalous plateau at high H/M (hydrogen-to-metal ratio) concentrations observed by Sakamoto et al.,[1] who postulated that the secondary plateau resulted from a precursory phase separation not detectable by x-ray diffraction. Since the anomalous plateau was not observed in the alloys tested in this study, the secondary plateau observed by Sakamoto et al. is most likely due to inhomogeneities resulting from an incomplete homogenization. The annealing treatments performed in this study were longer in duration, higher in temperature and more likely resulted in complete homogenization. If the anomalous plateau resulted from a precursory phase separation, which occurs after annealing, the anomalous plateau should have been observed in these alloys as well. Also none of the other alloys studied in this work show an anomalous plateau at the high H/M concentrations. Some of the isotherms show a peak at the beginning of the absorption plateau, see Figure 4 and Figure 7 - Figure 10. The peak is usually observed at the lower temperatures, but is also seen at higher temperatures, e. g. Figure 9. At first, the peak was thought to arise from not achieving equilibrium. But performing runs with a long hold time between aliquots showed no change in the presence of the peak. This peak is a real phenomenon, and its observation depends upon the size of the aliquot and the flattness of the plateaus. The peak in the isotherm can be explained as a hydride nucleation barrier. In other words, an over-pressure is required to first nucleate the hydride. Once the hydride has formed, the pressure required to grow the hydride is reduced. Large aliquots will miss the peak because the over-pressure will be exceeded during absorption and the measured equilibrium pressure will be less

than the peak pressure. Also isotherms which slope considerably will not show the peak. Since the alloys in this work have flat plateaus, it is more likely that the peak will be observed. This phenomonon will be investigated further in an upcoming paper.

The solution of hydrogen in the α phase at infinite dilution can be expressed as:

$$\tfrac{1}{2}H_2(g) + M \Leftrightarrow MH_\alpha \tag{1}$$

from which one obtains the thermodynamic relation[20]:

$$\begin{aligned}\Delta\mu_H &= \tfrac{1}{2}RT\ln p_{H_2} = \Delta H_H - T\Delta S_H \\ &= \Delta H_H^o - T\Delta S_H^o + RT\ln\left(\frac{r}{1-r}\right) + \mu_H^E(r)\end{aligned} \tag{2}$$

where $\Delta\mu_H$ is the relative chemical potential of hydrogen, μ_H^E is the excess chemical potential, ΔH_H° and ΔS_H° are the relative enthalpy and entropy of the solution of hydrogen at infinite dilution, and r is the hydrogen-to-metal ratio. Rearranging equation 2 gives:

$$\Delta\mu_H = RT\ln\left(\frac{p_{H_2}^{1/2}(1-r)}{r}\right) = \Delta\mu_H^o + \mu_H^E(r) \tag{3}$$

where $\Delta\mu_H^\circ$ is the relative chemical potential of dissolved hydrogen at infinite dilution. The excess chemical potential term vanishes in the limit of infinite dilution, i.e. as r → 0. Therefore plots of $\Delta\mu_H$ against r gives $\Delta\mu_H^\circ$ at r=0 and the non-ideal interaction term is obtained from the slope. The values of $\Delta\mu_H^\circ$ /T are then plotted against 1/T to obtain ΔH_H° and ΔS_H°. The results of these plots are given in Table 3. By comparing the ternary alloys containing a base 5% Rh content, increasing cobalt content decreases the enthalpy and entropy of the solution of hydrogen at infinite dilution. In other words, increasing the cobalt content increases the solubility of hydrogen at infinite dilution. As shown by Flanagan and Lynch[21], cold work, or in this case cycling, has a strong effect on the enthalpy and entropy of hydrogen at infinite dilution. So it is

not clear as to whether the effect of alloying on the enthalpy and entropy of hydrogen at infinite dilution results from a chemical effect or a mechanical effect. Future studies will aim at investigating the solution of hydrogen in annealed foils where the effect of dislocations is minimized.

The plateau chemical reaction can be written as:

$$\tfrac{1}{2}H_2(g) + \frac{1}{\beta-\alpha}MH_\alpha \Leftrightarrow \frac{1}{\beta-\alpha}MH_\beta \qquad (4)$$

where α and β are the solid solution α-phase and β-hydride phase boundary compositions at a given temperature. The thermodynamics can be determined by examining the temperature dependence of the plateau pressures for this reaction. The standard free energy change for β-hydride formation from the saturated α-phase with reference to $(\frac{1}{2})H_2$(1 atm, g) is given as[22]:

$$\Delta G_{plateau} = RT\ln p^{1/2} = \Delta H_{plateau} - T\Delta S_{plateau}. \qquad (5)$$

Van't Hoff plots of $\ln p^{1/2}$ against 1/T will produce the standard enthalpy change, ΔH_{plat}, and the standard entropy change, ΔS_{plat}. In this work, the plateau pressure used to obtain the thermodynamics is interpolated from the data and calculated at a hydrogen composition of H/M = 0.30. The absorption and desorption van't Hoff plots are presented in Figure 11 and Figure 12, respectively, and the enthalpy and entropy values are given in Table 3. Comparing alloys at a constant base 5% Rh concentration shows that the absolute value of the enthalpy of hydride formation and decomposition decreases with increasing Co content. Similarly, the enthalpy decreases with increasing Rh content in the alloys with no Co additions. As shown in Figure 13, the absorption enthalpy of the plateau reaction of the Pd-Rh, Pd-Co and Pd-Rh-Co alloys decreases linearly with a decreasing lattice parameter to 3.880 Å, where significant deviation from linearity occurs. This is all consistent with the concept that alloys, with contracted lattices

with respect to pure palladium, have a plateau enthalpy less than that of pure palladium. An interesting observation is that the plateau thermodynamics of the Pd-10Rh alloy and the Pd-5Rh-3Co alloy are quite similar and will consequently have similar plateau pressures. Therefore, it is possible, by ternary alloying with Co, to decrease the Rh content and still have an alloy with equivalent plateau thermodynamics. The standard entropy values do not show a strong effect of increasing Co content at a constant base 5% Rh content. Within the errors of the van't Hoff plots, the entropy values are relatively independent of alloying and are constant at about 42-43 J/K*mol.

A consistent measure of the capacity, which allows comparison between different alloys at a given temperature, is the β_{min} concentration. This is the composition of the β-hydride phase in equilibrium with the α-phase across the two-phase, plateau region. The β_{min} concentration is measured from the intersection of lines drawn parallel to the plateau and parallel to the β-phase solution data. At a constant 5% Rh content, the capacities, shown in Table 4, decrease with increasing Co content as would be expected from the results of the binary Pd-Co data[10]. Comparing Pd-10Rh and Pd-5Rh, the storage capacities are roughly the same; however adding 3% Co to the 5% Rh alloy decreases the capacity by 0.09 H/M due to the strong effect of Co on reducing the capacity. Therefore, provided that the reduction in capacity can be tolerated, the Pd-5Rh-3Co alloy could possibly replace the Pd-10Rh alloy if phase separation was an issue.

3.3 Dilute solution model based on binary alloys

As mentioned previously, no known attempts have been made to model alloy design of Pd alloys for hydrogen storage. Since the lattice parameter measurements show a linear dependence upon concentration, Figure 2 and Sakamoto et al.[23], and the total alloying contents

are kept less than 10%, it reasonable to assume that the alloys of interest behave as dilute ideal solutions. In fact, the lattice parameters of the binary and ternary alloys are in close agreement with the values calculated using Vegard's Law, as seen in Table 2. Therefore, the thermodynamic parameters should also follow a dilute ideal solution behavior. The enthalpy and entropy of hydride formation/decomposition will then be linearly dependent on both the alloy content and alloying element. The absorption thermodynamic properties for Pure Pd are from Sakamoto et al. [1] and the desorption properties are from Frieske et al.[24]. Using the thermodynamic parameters presented above for cycled Pd-Rh and Pd-Co alloys and from the measurements of Wang et al. for the Pd-Co alloys[10], a linear fit can be made to the thermodynamic parameters of the binary alloys as a function of alloying element and concentration. The ternary alloy system can then be modeled as a linear superposition of the binary equations, and is given below:

$$\Delta H_f^{plateau} = 18.4 - 0.5*(\%Rh) - 0.6*(\%Co) \quad (6a)$$

$$\Delta H_d^{plateau} = 20.5 - 0.4*(\%Rh) - 0.5*(\%Co) \quad (6b)$$

$$\Delta S_f^{plateau} = 45.5 - 0.2*(\%Rh) - 0.4*(\%Co) \quad (7a)$$

$$\Delta S_d^{plateau} = 48.7 + 0.2*(\%Rh) + 0.2*(\%Co) \quad (7b)$$

As seen in equation 6, cobalt has a stronger effect on the enthalpy for hydride formation/decomposition than does rhodium. Similarly cobalt has a stronger effect on the entropy for hydride formation; whereas rhodium and cobalt produce equivalent changes in the entropy for hydride decomposition. This is evident by comparing the PC curves for the binary Pd-Rh alloys to the binary Pd-Co alloys. For equal alloying contents, cobalt increases the plateau pressures greater than rhodium. This effect can be most likely explained as a size effect since

cobalt has a stronger effect on the lattice parameter than rhodium. If cobalt contracts the lattice more than rhodium, the pressures required to produce the hydride phase would be expected to be higher due to the large volume expansion associated with the hydride.

A similar approach can be used to model the storage capacity of these alloys. For comparison, β_{min} is measured at 50 °C; and the model is also fit for 50°C. The data for the Pd-Co system was obtained from our data and data from Wang et al.[10]. The capacities of the Pd-Co alloys followed a linear dependence as a function of Co content. The Pd-Rh data acquired in this work was used to fit the dependence of β_{min} on the Rh content. A parabolic fit was used in the Pd-Rh case since a maximum in β_{min} is observed at about 7 %Rh. By superimposing these two relations, one obtains:

$$\beta_{\min} = 0.61 + 7.0 \cdot 10^{-3} \cdot (\%Rh) - 4.5 \cdot 10^{-4} \cdot (\%Rh)^2 - 2.8 \cdot 10^{-2} \cdot (\%Co) \qquad (8)$$

as the dependence of the capacity on the alloying contents for the ternary Pd-Rh-Co alloys. Cobalt has a strong effect on the capacity of the Pd-Rh alloys, and therefore its additions to the Pd-Rh binaries must be limited to still retain sufficient capacity for a useful alloy in hydrogen storage.

Using the equations (6-7) expressed above, we can predict the thermodynamic parameters of the ternary alloys and subsequently the plateau pressures as a function of temperature. A comparison of the calculated and measured values for the enthalpy and entropy of hydride formation/decomposition is given in Table 4. Fairly good agreement of the enthalpy values exists for most of the alloys. Less correlation is observed between the measured and calculated values for the entropy. However, the trends in the values are still valid. At a constant Rh content, additions of Co decrease the enthalpy and decrease the entropy of hydride formation and

decomposition. Figure 14 shows the calculated and measured absorption plateau pressures for Pd-5Rh-XCo alloys at 50°C. The agreement between the calculated and measured plateau pressures is best at low alloy contents. Ternary alloys containing greater than 6% total alloy content begin to show less agreement between the predicted and measured values. This may be indicating the limit of the dilute solution approximation. The alloys, which agreed best with the calculated values, were tested at four temperatures, giving a better statistical fit. Perhaps testing the alloys at more temperatures will yield better results. However, this ternary model is still useful as a guide to optimally design a higher-order Pd-based alloy for hydrogen storage.

The measured capacities, β_{min}, of the ternary Pd-Rh-Co alloys agree with the values calculated from equation (8) to within 0.01 H/M as seen in Table 4. The calculated capacities use the actual alloy concentration, not the nominal composition. This verifies that the additive superposition of the hydride thermodynamic properties is valid at least in dilute ternary and possibly higher-order alloys.

4. Conclusions

The main conclusions of this work are that:

- Purity and composition must be documented
- Alloys must be well characterized
- This leads to a viable model with good predictive capabilities

Our results have shown that the hydriding thermodynamics and hydrogen storage capacity of ternary alloys can be accurately predicted using a dilute solution approach, which interpolates the ternary space from existing binary data. This approach could very well be applied to higher-order dilute alloys as well. The main reason, for duplicating some of the binary alloy work that has

been previously presented in the literature, was that the purity, actual compositions and microstructure can strongly affect the PCT behavior. Full characterization of the alloy is important when trying to model binary and ternary PCT behavior. Knowing the actual compositions, as well as interstitial content, is paramount to achieve a good fit. The major impact of this model is that the thermodynamic properties can be tailored for a specific application through ternary and possibly higher-order alloying. Pressure-composition-temperature behaviors not previously achievable in binary alloys can be developed with ternary and higher-order dilute alloys. Efforts are ongoing to determine whether the dilute solution and solvus thermodynamics can be modeled in a similar approach. Also other ternary systems will be studied to verify the generality of this model.

5. Acknowledgements

The authors wish to thank the assistance of Mike Mauro and Ann Kelly in the preparation and characterization of the alloys. This work was supported under DOE Contract No. W-7405-ENG-36.

References

1. Y. Sakamoto, et al., *Ber. Bunsenges. Phys. Chem.*, 1994, **98,** p. 964-969.

2. K. Watanabe, et al., *Scripta Materialia*, 1996, **34,** p. 551-557.

3. R. D. Field and D. J. Thoma, *Scripta Materialia*, 1997, **37,** p. 347-353.

4. H. Noh, et al., *Scripta Met. Mater.*, 1991, **25,** p. 225-230.

5. H. Noh, et al., *J. Alloys Compounds*, 1996, **240,** p. 235-248.

6. R. Gurler, et al., *J. Alloys Comp.*, 1993, **191,** p. 165-168.

7. E. Raub, et al., *Z. Metallkde.*, 1959, **50,** p. 428-431.

8. J. E. Shield and R. K. Williams, *Scripta Met.*, 1987, **21,** p. 1475-1479.

9. Y. Matsuo, *J. Phys. Soc. Japan*, 1972, **32,** p. 972-978.

10. D. Wang, et al., *J. Alloys Comp.*, 1997, **252,** p. 209-218.

11. R. Feenstra, et al., *J. Less Comm. Metals*, 1987, **130,** p. 375-386.

12. K. Ohira, et al., *J. Alloys Compounds*, 1996, **236,** p. 42-49.

13. Y. Sakamoto, et al., *J. Alloys Compounds*, 1995, **217,** p. 226-234.

14. A. Weiss, et al., *Z. Phys. Chem.*, 1997, **199,** p. 165-212.

15. Y. Sakamoto, et al., *Z. Phys. Chem. Neue Folge*, 1989, **162,** p. 83-96.

16. S. Müller and P. Scholten, *Z. Ange. Physik*, 1966, **20,** p. 498-502.

17. R. Kohlhaas, et al., *Z. Ange. Physik*, 1967, **23,** p. 245-249.

18. G. I. Kulesko and A. L. Seryugin, *Physics of Metals and Metallogrpahy*, 1968, **26,** p. 140-143.

19. R. G. Ross and W. Hume-Rothery, *J. Less Common Metals*, 1963, **5,** p. 258-270.

20. W. A. Oates and T. B. Flanagan, *J. Mater. Sci.*, 1981, **16,** p. 3235-3243.

21. T. B. Flanagan and J. F. Lynch, *J. Less Common Metals*, 1976, **49,** p. 13-24.

22. T. B. Flanagan and J. F. Lynch, *J. Phys. Chem.*, 1975, **79,** p. 444-448.

23. Y. Sakamoto, et al., *Z.Phys. Chem. N.F.*, 1988, **158,** p. 223-235.

24. E. Wicke and H. Brodowsky, in Hydrogen in Metals II: Application - Oriented Properties, Vol. 29, edited by G. Alefeld and J. Völkl (Springer - Verlag, New York, 1978), p. 73-156.

Table 1: Results of the chemical analysis of the alloys used in this study. A dashed line indicates that the element was below the level of detectability given in the last row.

	(at.%)			(appm)					
Alloy	**Pd**	**Rh**	**Co**	**B**	**C**	**N**	**O**	**S**	**P**
Pd	99.97	0.01	---	---	---	---	166	---	---
Pd5Rh	95.17	4.75	---	98	---	---	126	---	---
Pd10Rh	90.65	9.27	---	---	---	---	186	---	---
Pd2Co	97.87	0.01	2.02	---	439	---	244	---	---
Pd5Co	95.49	0.01	4.42	---	434	---	46	65	---
Pd9Co	90.05	0.01	9.87	---	423	---	51	---	---
Pd5Rh1Co	93.92	4.80	1.02	---	2108	---	237	---	---
Pd5Rh3Co	92.11	4.75	3.04	---	436	---	229	---	---
Pd5Rh5Co	89.82	4.97	5.12	---	---	---	143	32	---
Pd4Rh2Co	94.06	3.76	2.09	---	---	---	151	---	---
Detectability		0.001	0.002	98	420	75	33	32	102

Table 2: Microstructural variables measured for the alloys studied in this work.

Alloy	Lattice Parameter, a_{ss} (nm)		Grain Size (μm)	Hardness (VHN)		Thickness (μm)
	Calculated	Measured		Annealed	Cycled	
Pd	---	3.8901±0.0003		63.7	---	
Pd5Rh	3.886	3.8874±0.0003	65	70	132	89
Pd10Rh	3.882	3.8815±0.0004	59	83	136	96
Pd2Co	3.883	3.8865±0.0005	136	70	---	112
Pd5Co	3.875	3.8812±0.0001	140	76	119	110
Pd9Co	3.856	3.8724±0.0002	109	76	117	83
Pd5Rh1Co	3.882	3.8849±0.0001	54	67	116	96
Pd5Rh3Co	3.875	3.8817±0.0003	50	62	127	96
Pd5Rh5Co	3.868	3.8765±0.0001	54	82	128	106
Pd4Rh2Co	3.880	3.8828±0.0002	45	75	123	118

Table 3: A summary of the thermodynamic properties of the binary and ternary Pd-Rh-Co alloys. [(a)] Reference [1] and [(b)] reference [24].

			Absorption		Desorption	
	ΔH_H^o	ΔS_H^o	ΔH^{plat}	ΔS^{plat}	ΔH^{plat}	ΔS^{plat}
Alloy	**(kJ/mol H)**	**(J/K*mol H)**	**(kJ/mol H)**	**(J/K*mol H)**	**(kJ/mol H)**	**(J/K*mol H)**
Pd	---	---	-18.4[(a)]	45.5[(a)]	20.5[(b)]	-48.7[(b)]
Pd5Rh	-10.5±1.6	57.9±5.1	-17.0±0.3	47.2±1.0	19.1±0.2	-50.8±0.6
Pd10Rh	-10.2±0.1	61.6±0.4	-13.7±0.1	42.5±0.4	16.7±0.1	-50.2±0.2
Pd5Co	-8.1±1.7	51.3±5.1	-14.6±0.5	40.4±1.5	19.1±0.1	-52.3±0.3
Pd9Co	-8.0±0.5	56.1±1.7	-13.1±0.3	42.2±0.8	15.5±0.1	-49.1±0.3
Pd5Rh1Co	-10.2±0.5	57.8±1.4	-15.3±0.2	43.7±0.6	19.3±0.1	-53.2±0.2
Pd5Rh3Co	-8.0±0.1	53.4±0.4	-13.8±0.1	41.7±0.2	17.3±0.2	-50.8±0.8
Pd5Rh5Co	-6.1±0.1	50.5±0.4	-13.2±0.3	42.5±1.1	16.3±0.1	-51.0±0.1
Pd4Rh2Co	-10.4±0.7	59.0±2.1	-15.1±0.1	43.4±0.4	19.0±0.1	-52.7±0.2

Table 4: Comparison of calculated and measured plateau thermodynamic parameters. Values with and without parentheses correspond to calculated and measured properties, respectively. Calculated values use the actual alloy composition from **Table 1**.

Alloy		ΔH°_{plat} *(kJ/mol H)*		ΔS°_{plat} *(J/(K*mol H)*		β_{min} *(H/M) @ 50 °C*	
X_{Rh}	X_{Co}	*absorption*	*desorption*	*absorption*	*desorption*	*calculated*	*measured*
5	0	-17.0 (-16.0)	19.1 (18.6)	47.2 (44.6)	-50.8 (-49.7)	0.63	0.63
5	1	-15.3 (-15.4)	19.3 (18.1)	43.7 (44.1)	-53.2 (-49.9)	0.60	0.62
5	3	-13.8 (-14.2)	17.3 (17.1)	41.7 (43.3)	-50.8 (-50.3)	0.55	0.55
5	5	-13.2 (-12.8)	16.3 (16.0)	42.5 (42.5)	-51.0 (-50.7)	0.49	0.49
4	2	-15.1 (-15.3)	19.0 (18.0)	43.4 (43.9)	-52.7 (-49.9)	0.57	0.58
10	0	-13.7 (-13.8)	16.7 (16.8)	42.5 (43.6)	-50.2 (-50.6)	0.64	0.64

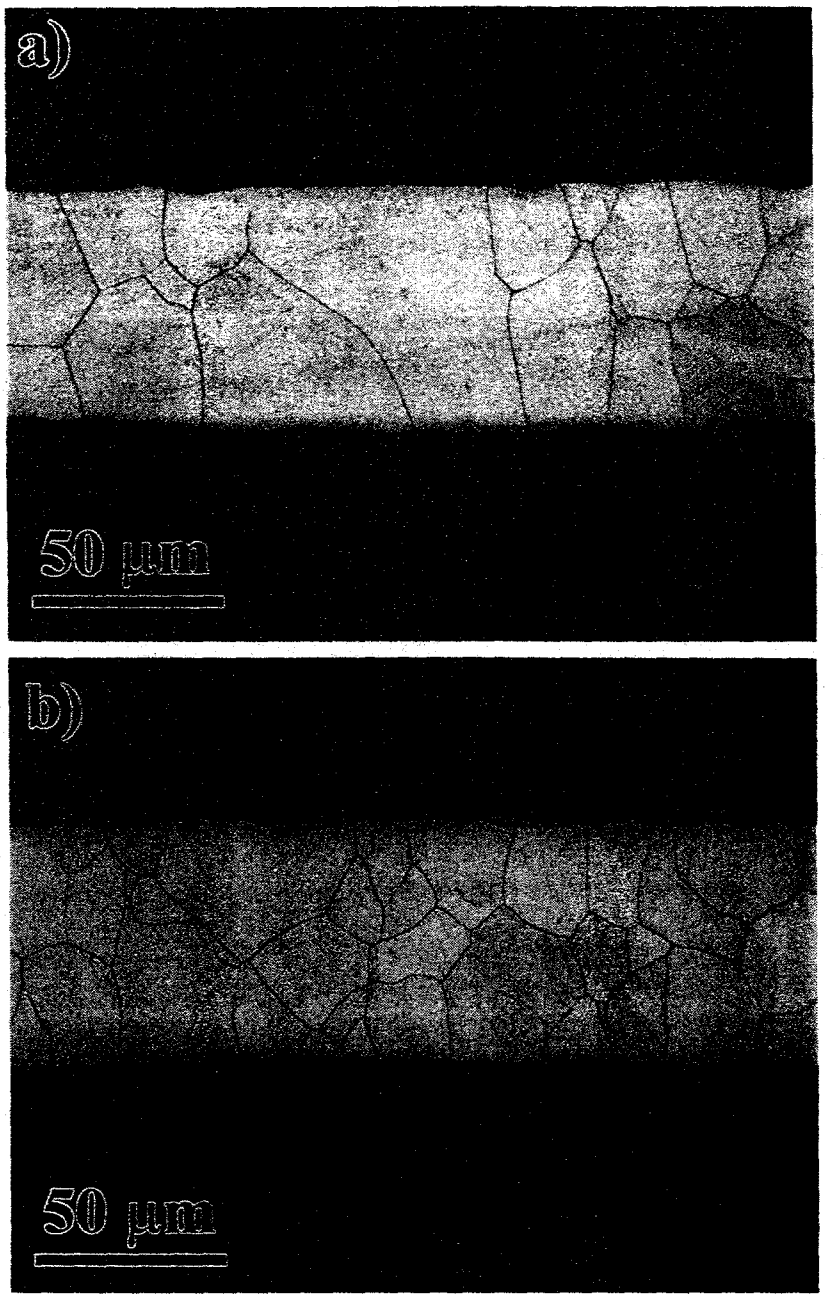

Figure 1: Optical micrographs of the annealed foils of (a) Pd-5Rh-1Co and (b) Pd-4Rh-2Co.

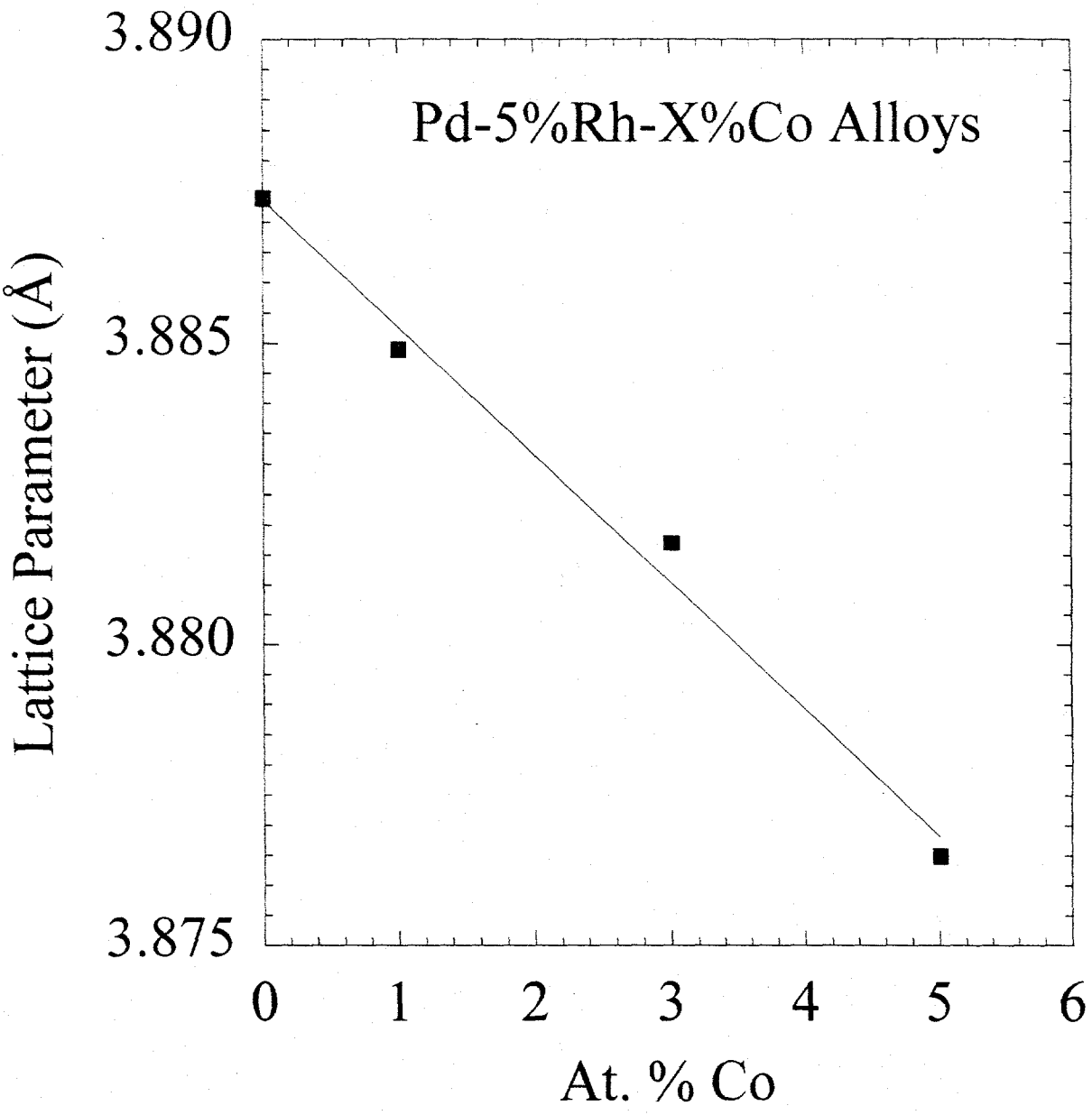

Figure 2: Measured lattice parameters of Pd-5%Rh-X%Co alloys showing a linear dependence of the lattice parameter on increasing Co content.

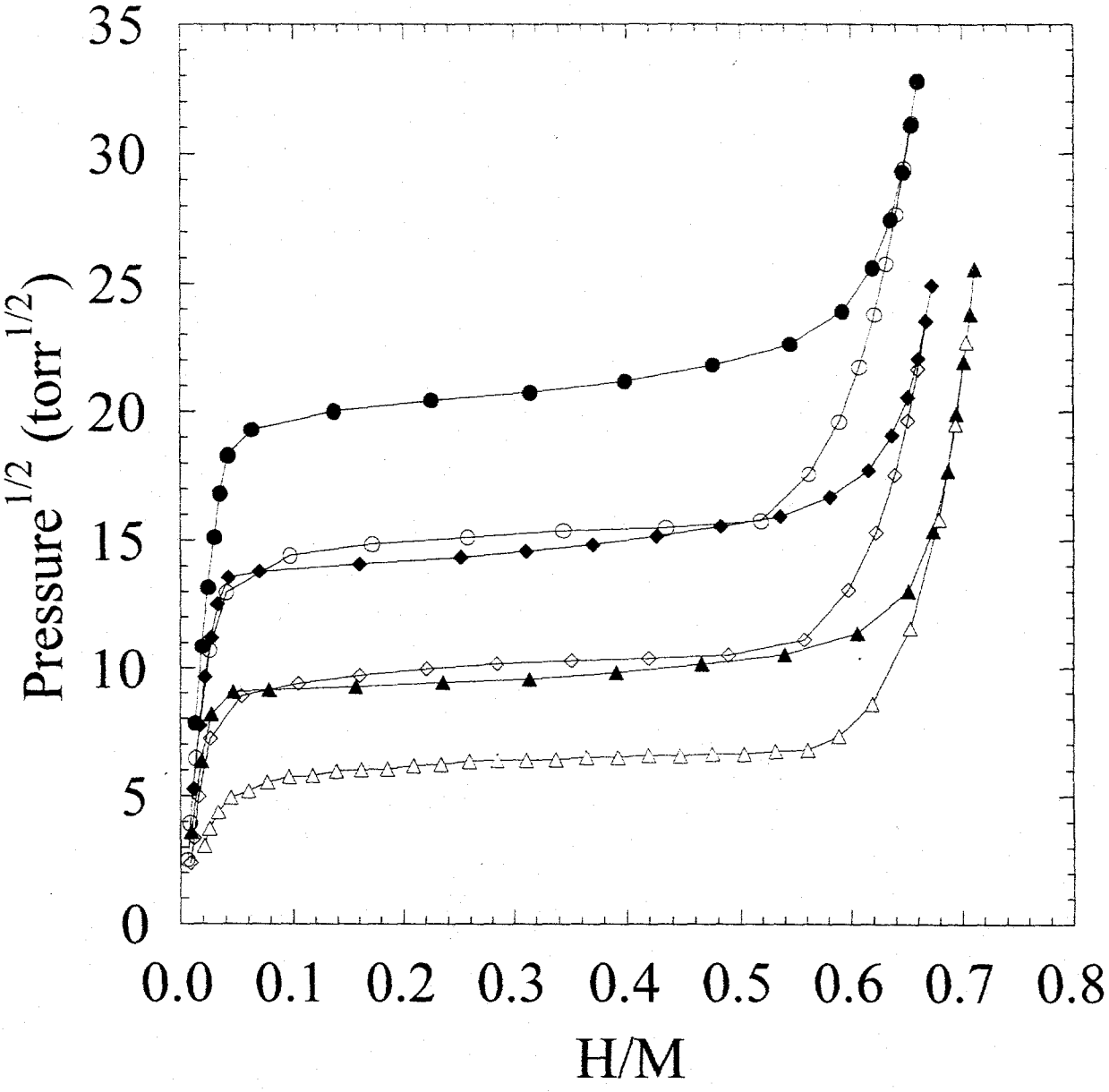

Figure 3: Isotherms for Pd-5Rh at 30°C (▲), 50°C (◆), and 70°C (●). Absorption curves are filled symbols and desorption curves are open symbols.

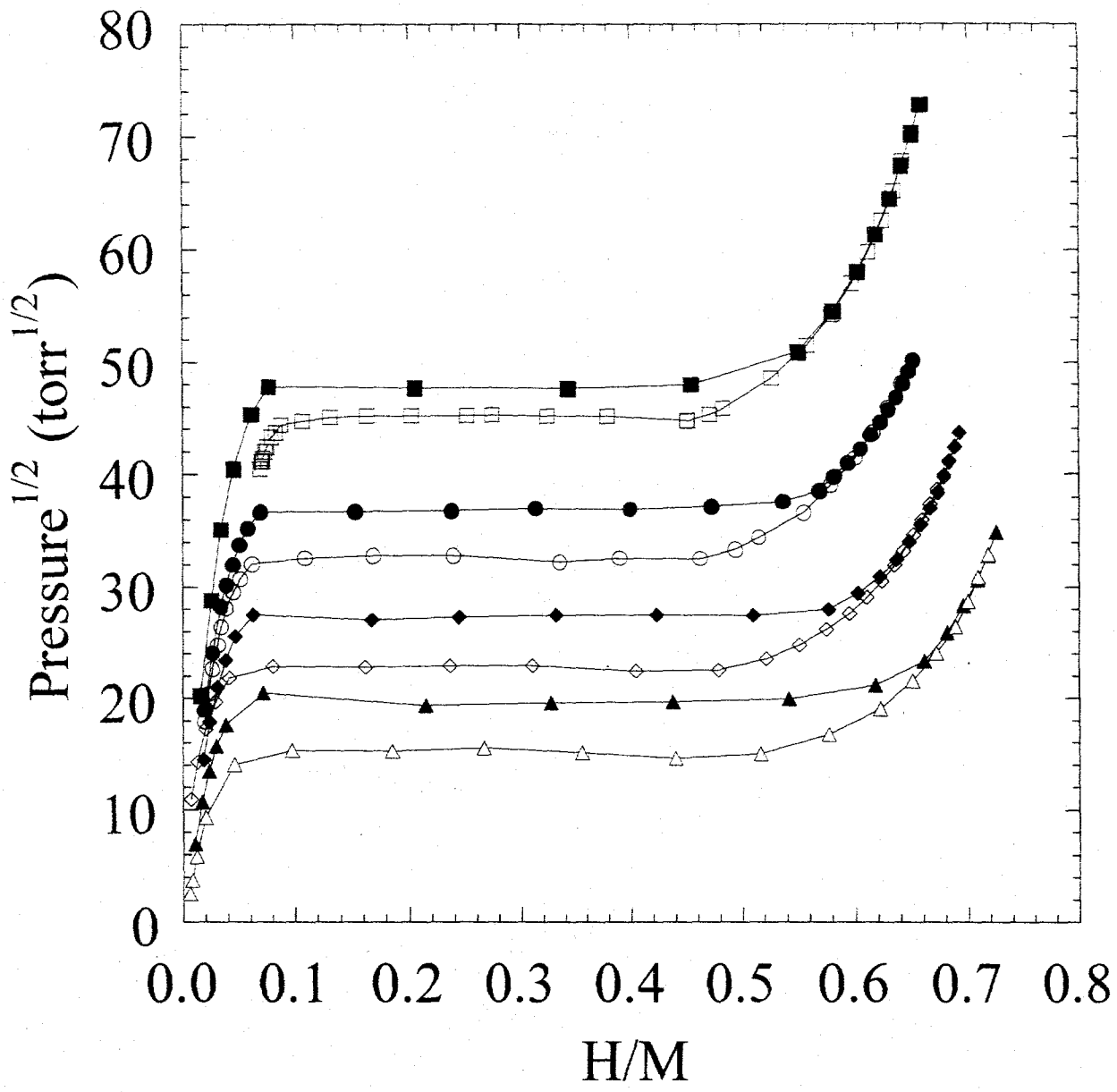

Figure 4: Isotherms for Pd-10Rh at 30°C (▲), 50°C (◆), 70°C (●) and 90°C (■). Absorption curves are filled symbols and desorption curves are open symbols.

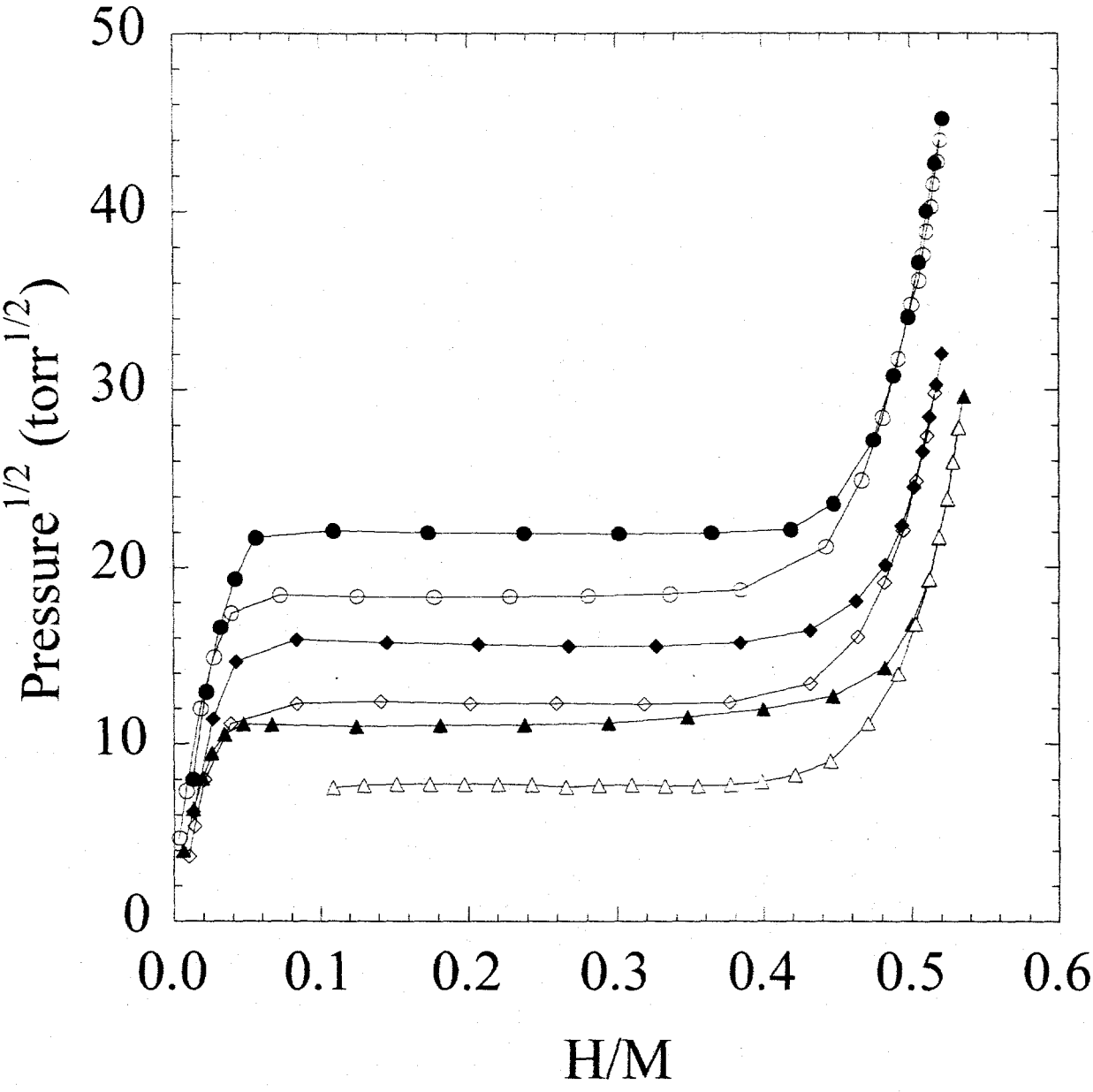

Figure 5: Isotherms for Pd-5Co at 30°C (▲), 50°C (◆), and 70°C (●). Absorption curves are filled symbols and desorption curves are open symbols.

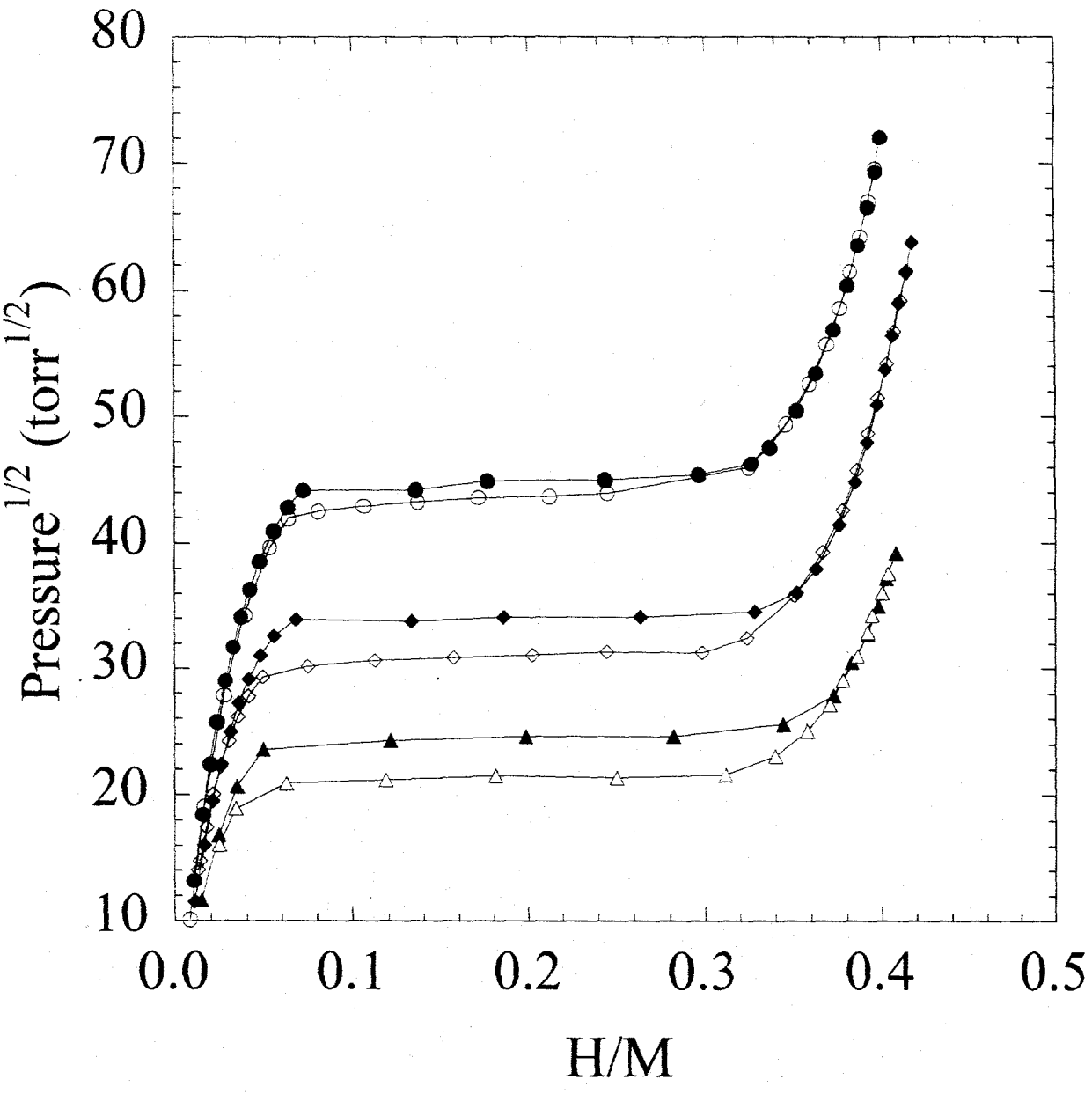

Figure 6: Isotherms for Pd-9Co at 30°C (▲), 50°C (◆), and 70°C (●). Absorption curves are filled symbols and desorption curves are open symbols.

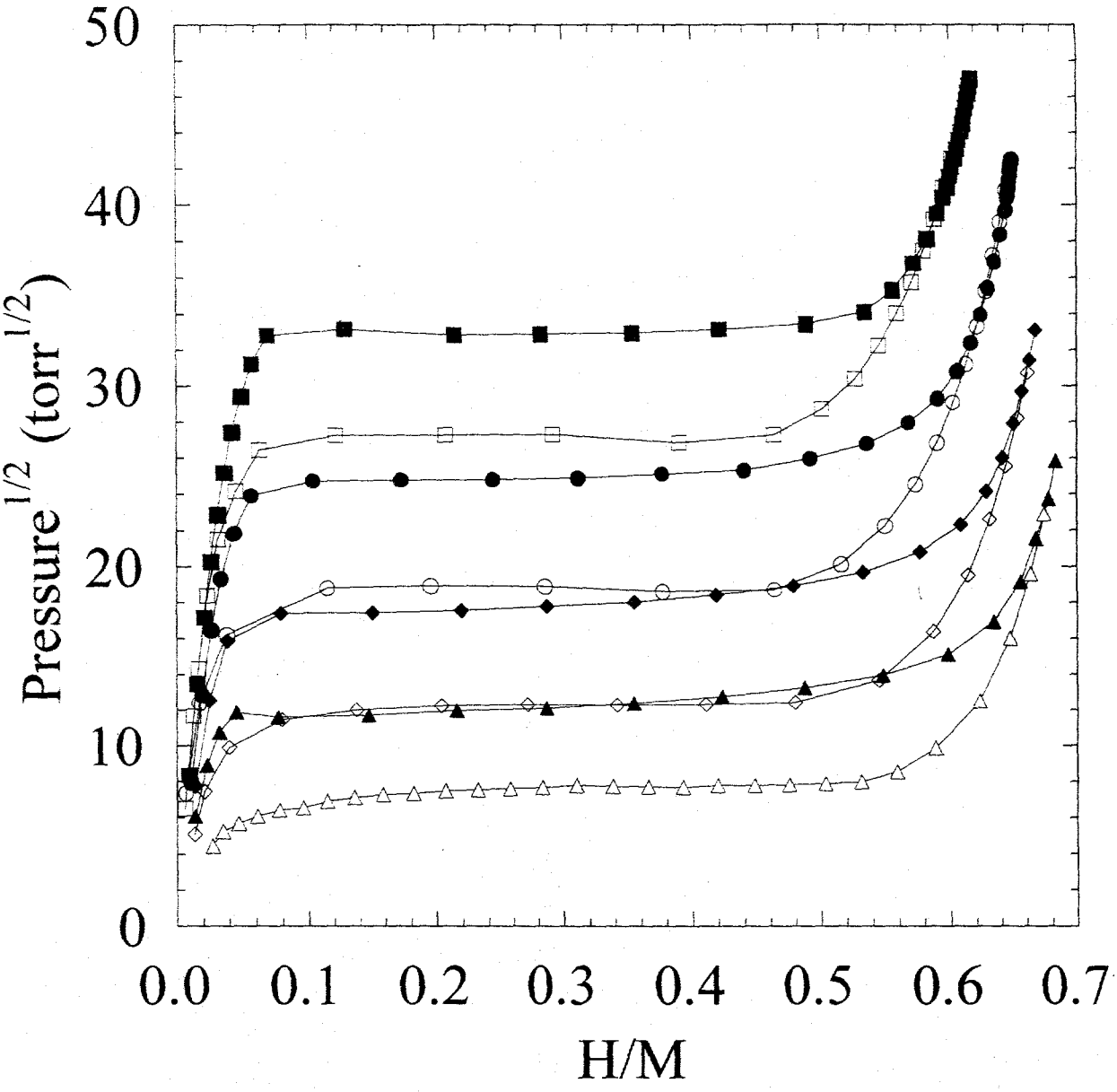

Figure 7: Isotherms for Pd-5Rh-1Co at 30°C (▲), 50°C (◆), 70°C (●) and 90°C (■).

Absorption curves are filled symbols and desorption curves are open symbols.

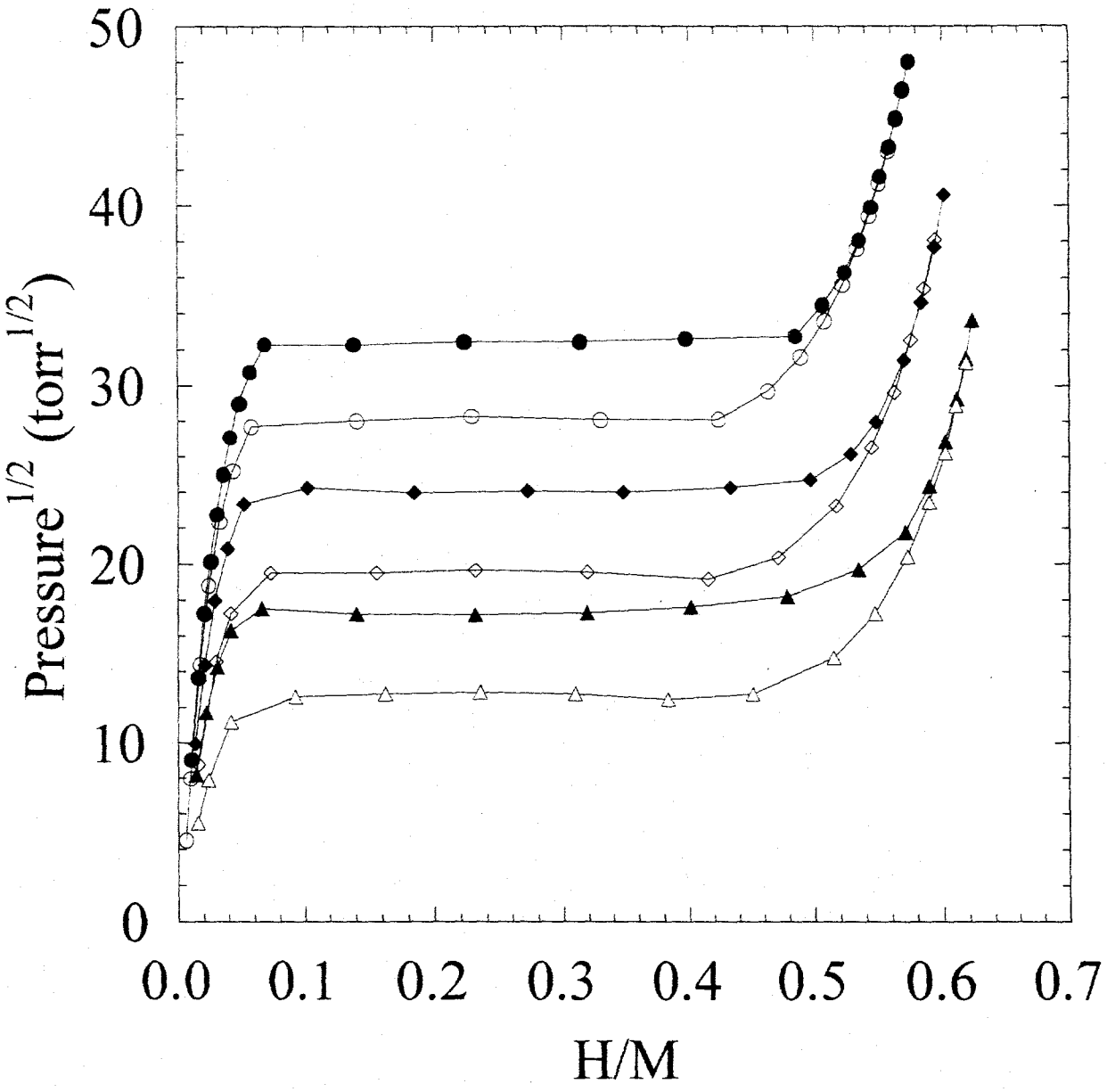

Figure 8: Isotherms for Pd-5Rh-3Co at 30°C (▲), 50°C (◆), and 70°C (●). Absorption curves are filled symbols and desorption curves are open symbols.

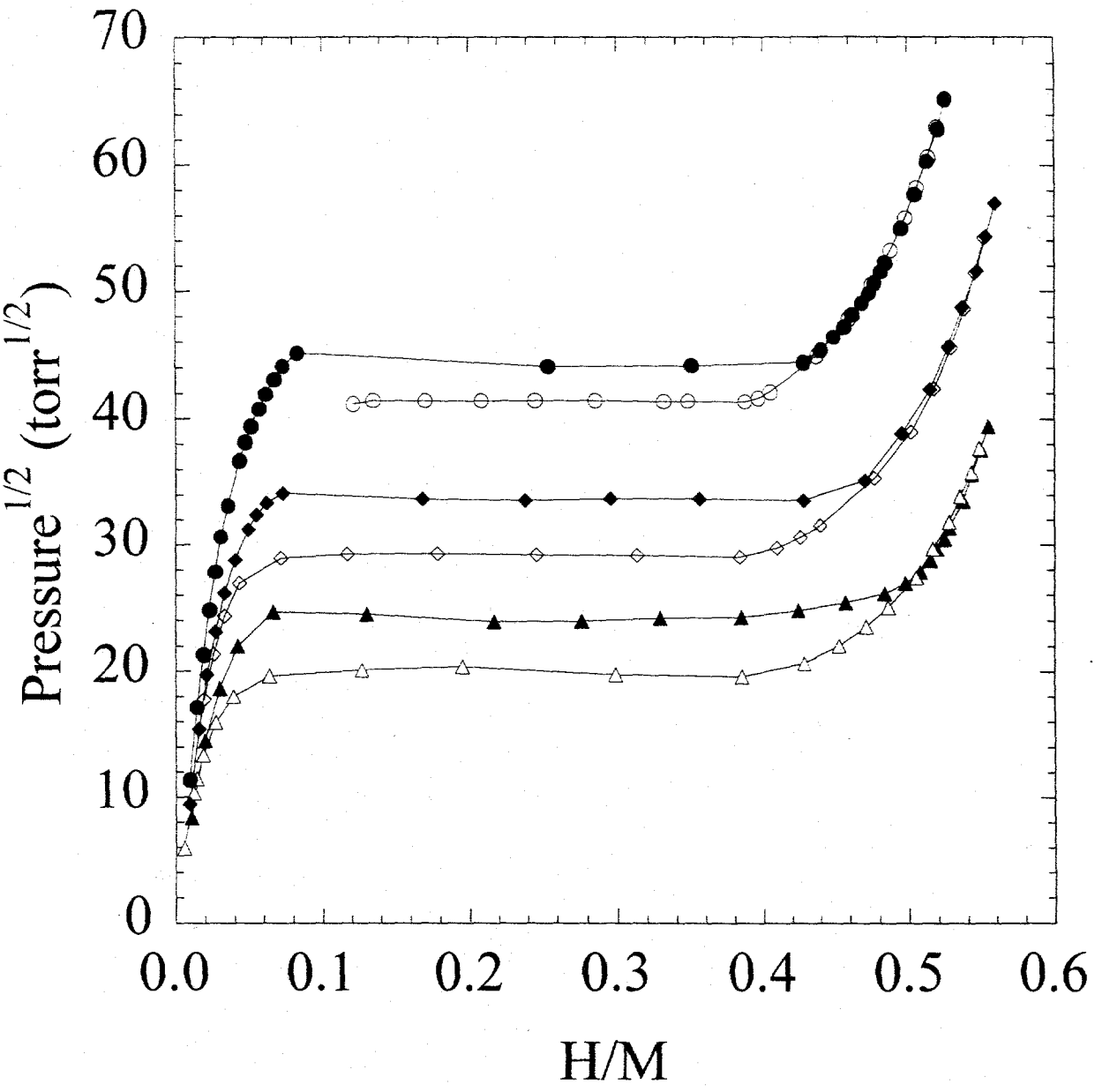

Figure 9: Isotherms for Pd-5Rh-5Co at 30°C (▲), 50°C (◆), and 70°C (●). Absorption curves are filled symbols and desorption curves are open symbols.

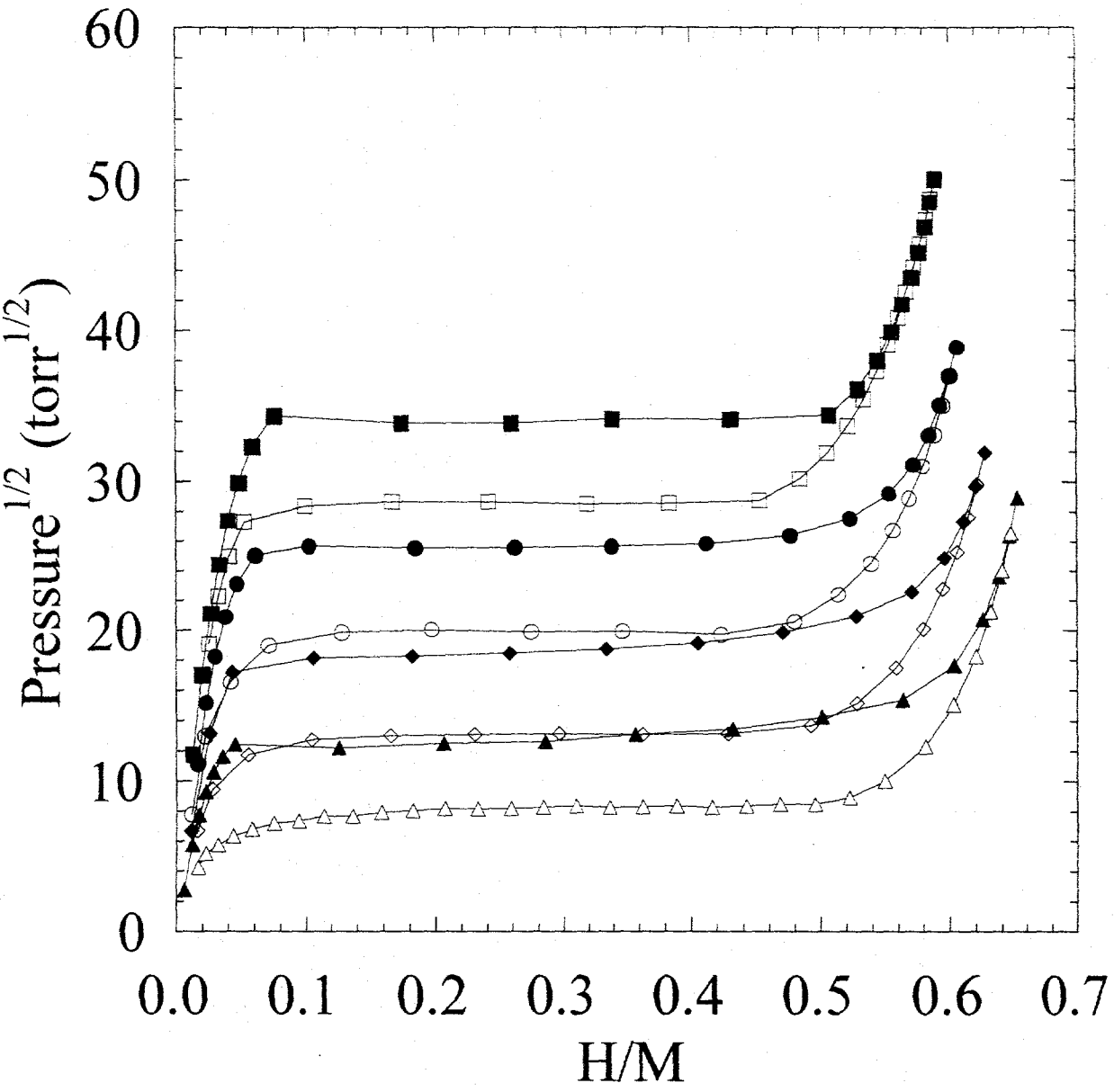

Figure 10: Isotherms for Pd-4Rh-2Co at 30°C (▲), 50°C (◆), 70°C (●) and 90°C (■).

Absorption curves are filled symbols and desorption curves are open symbols.

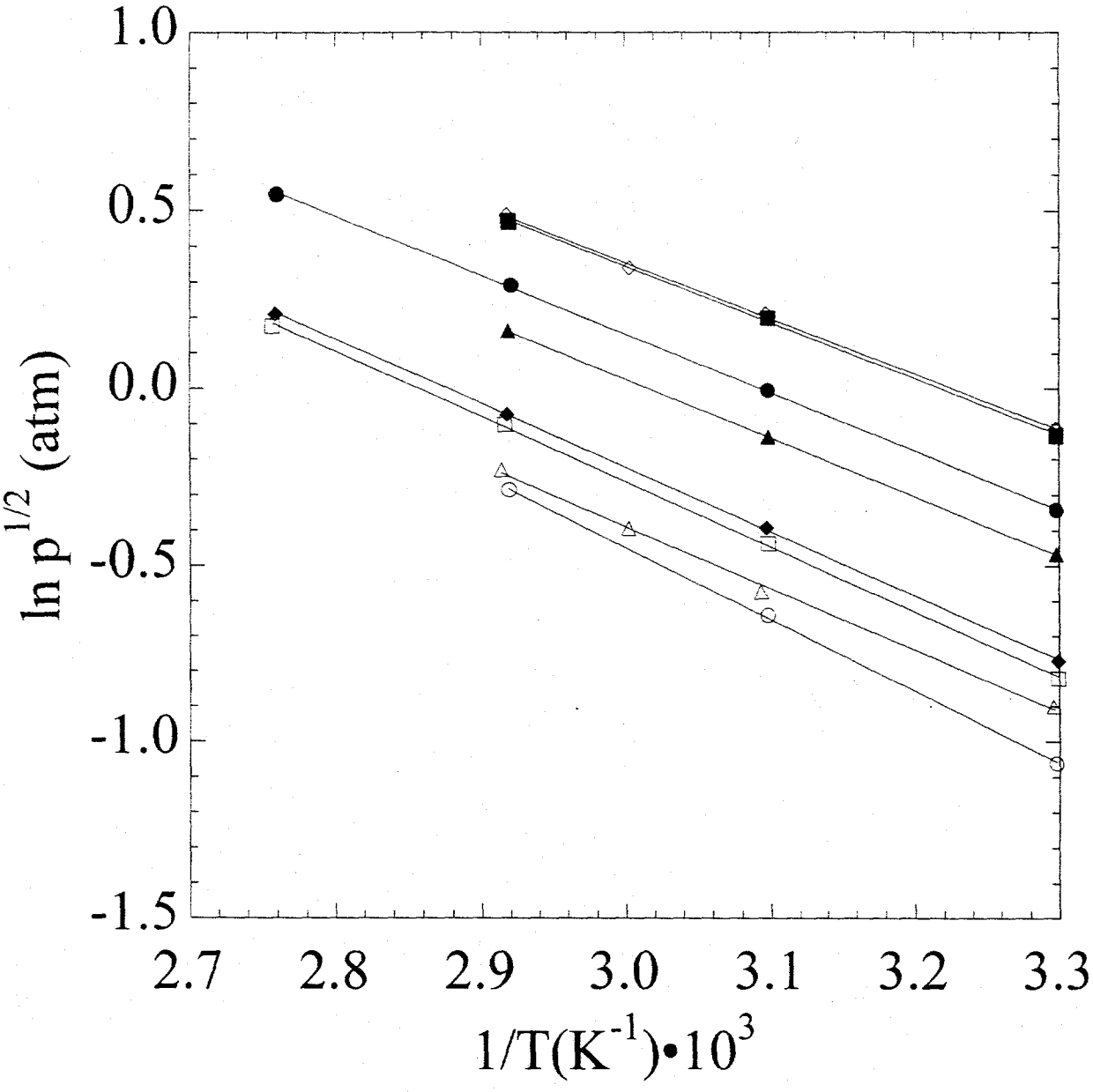

Figure 11: Van't Hoff plots of the absorption, hydriding data for Pd-9Co (◇), Pd-5Rh-5Co (■), Pd-10Rh (●), Pd-5Rh-3Co (▲), Pd-4Rh-2Co (◆), Pd-5Rh-1Co (□), Pd-5Co (△), and Pd-5Rh (○).

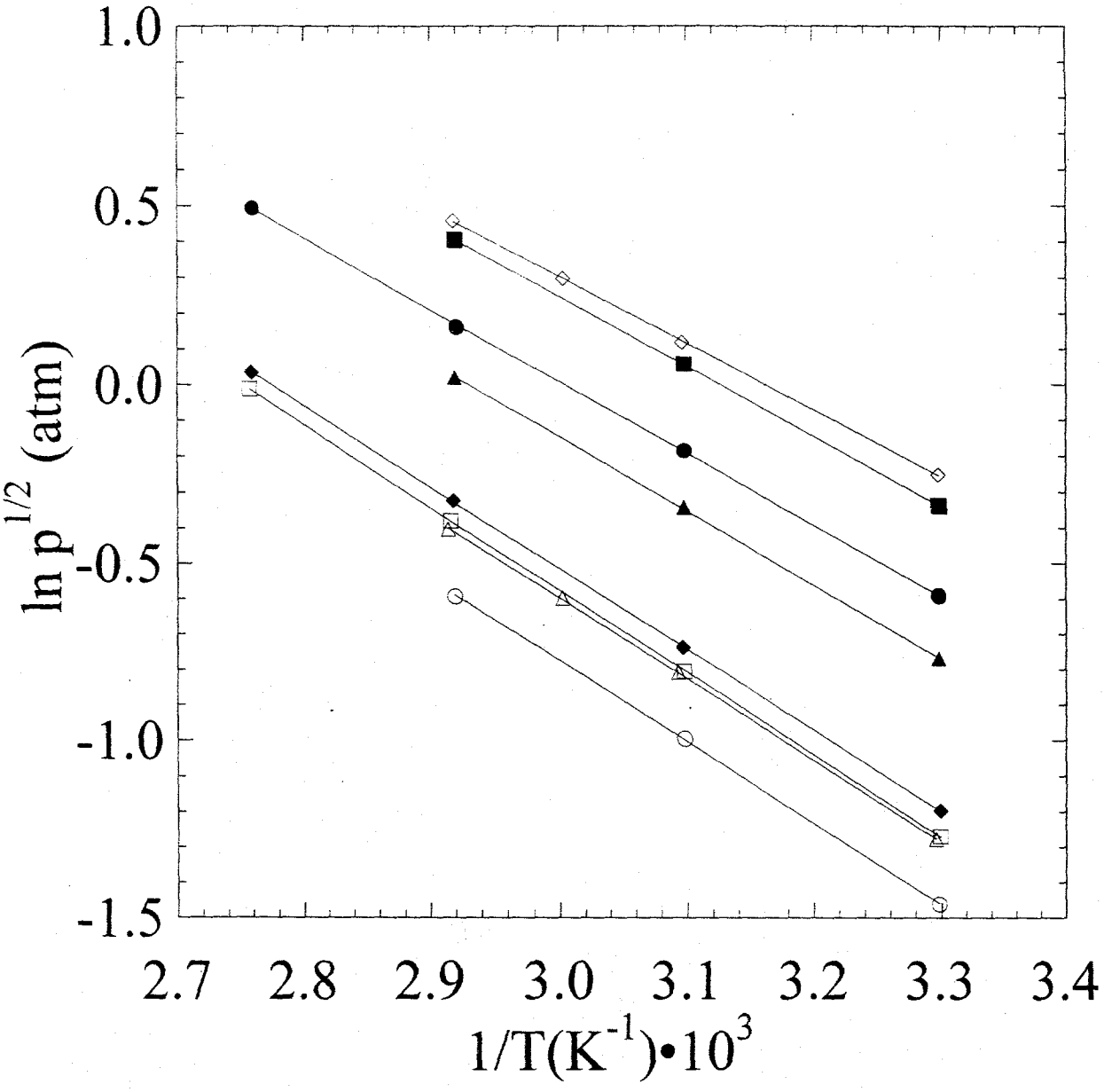

Figure 12: Van't Hoff plots of the desorption, dehydriding data for Pd-9Co (◇), Pd-5Rh-5Co (■), Pd-10Rh (●), Pd-5Rh-3Co (▲), Pd-4Rh-2Co (◆), Pd-5Rh-1Co (□), Pd-5Co (△), and Pd-5Rh (○).

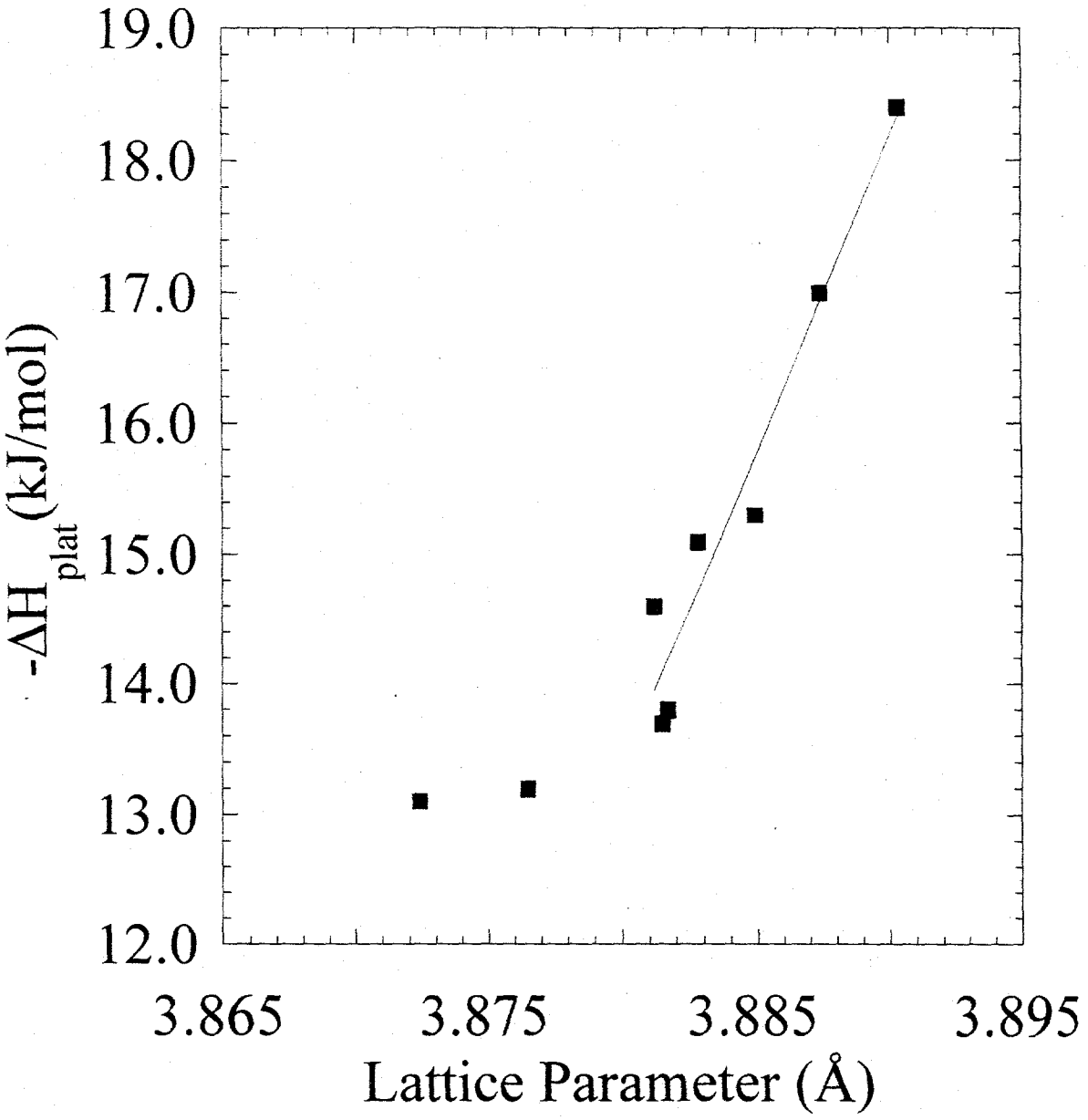

Figure 13: The correlation of lattice parameter with the enthalpy of hydride formation in Pd-Rh and Pd-Rh-Co alloys.

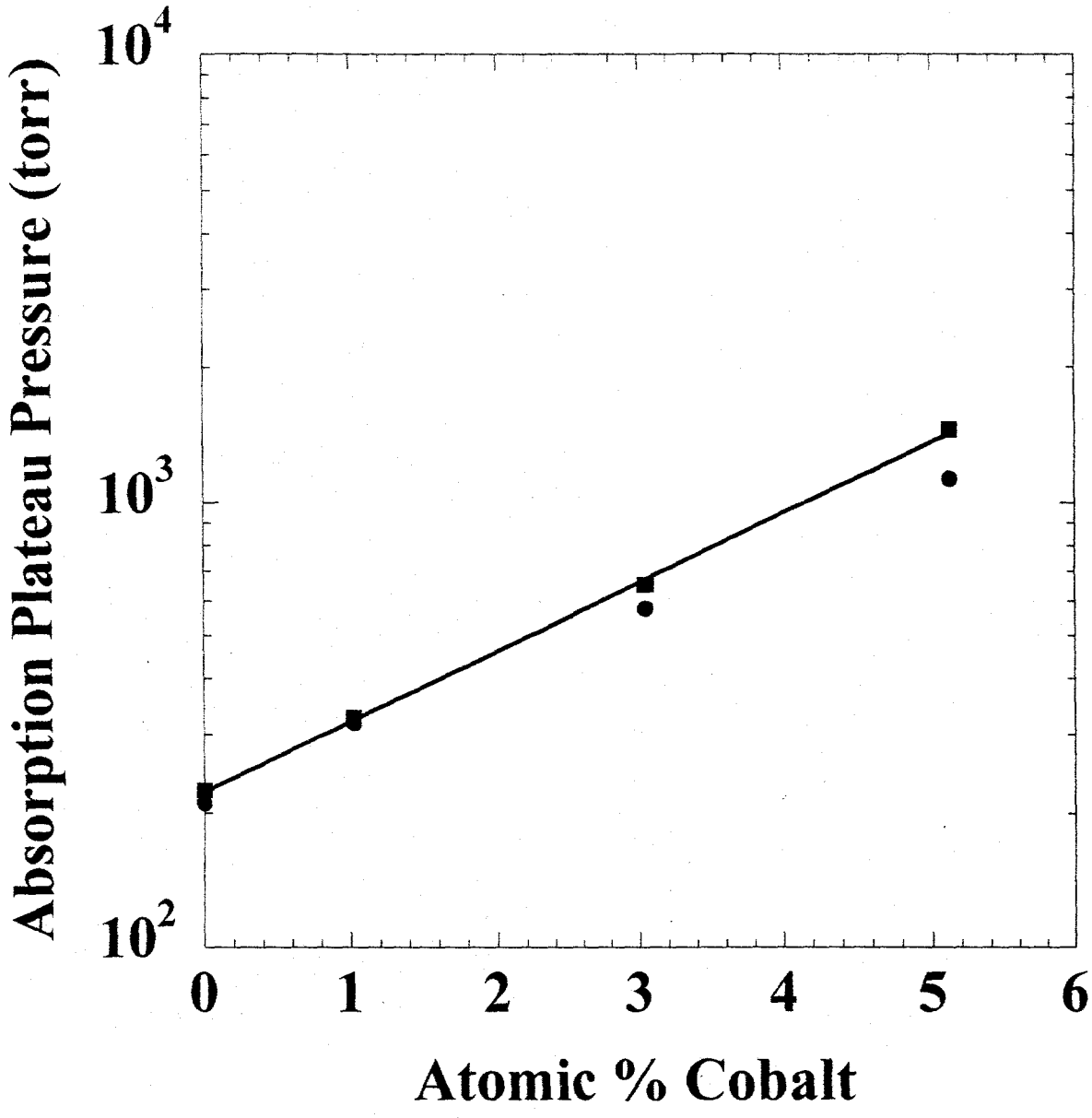

Figure 14: Comparison between the calculated (■) and measured (●) absorption plateau pressures at 50 °C for Pd-5Rh-XCo alloys.